Journal of the Korean Electrochemical Society
Vol. 27, No. 1, 2024, 15-31
https://doi.org/10.5229/JKES.2024.27.1.15

Supplementary
pISSN 1229-1935
eISSN 2288-9000

Electrochemical Detection of Hydroxychloroquine Sulphate Drug using CuO/GO Nanocomposite Modified Carbon Paste Electrode and its Photocatalytic Degradation

G. S. Shaila, Dinesh Patil, Naeemakhtar Momin, and J. Manjanna*
Dept. of Chemistry, Rani Channamma University, Belagavi 591156, Karnataka, India

(Received July 6, 2023 : Revised December 1, 2023 : Accepted December 13, 2023)

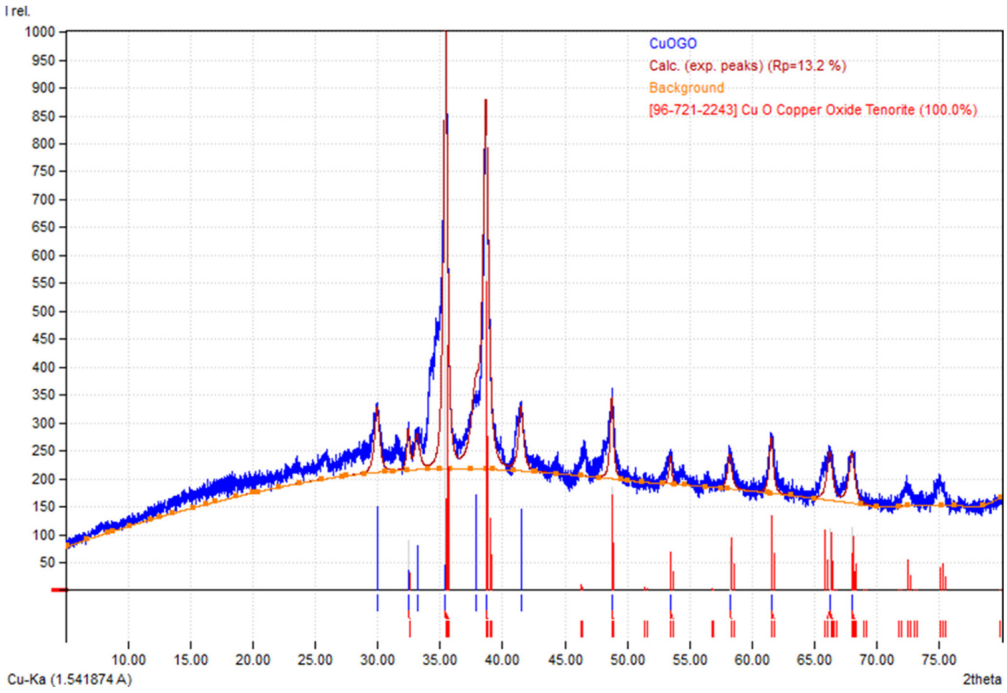

Fig. S1. XRD pattern of CuO/GO NC after Rietveld refinement using Match! supported Full proof Software.

*E-mail: jmanjanna@gmail.com

Match! Phase Analysis Report

Sample: CuOGO

Sample Data

File name	CuOGO.dat
File path	C:/Users/acer/Downloads
Data collected	Sep 6, 2023 13:59:53
Data range	5.000° - 79.990°
Original data range	5.000° - 79.990°
Number of points	7500
Step size	0.010
Rietveld refinement converged	No
Alpha2 subtracted	No
Background subtr.	No
Data smoothed	No
Radiation	X-rays
Wavelength	1.541874 Å

Analysis Results

Phase composition (Weight %)

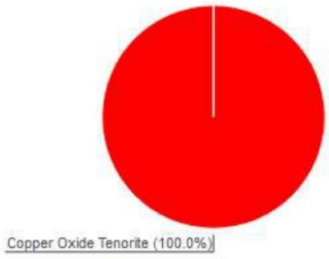

Elemental composition (Weight %)

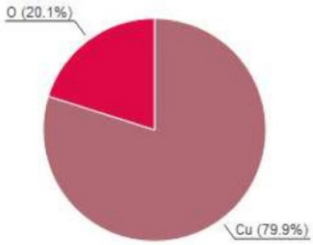

Index	*Amount (%)*	*Name*	*Formula sum*
A	100.0	Copper Oxide Tenorite	Cu O
	9.8	*Unidentified peak area*	

Element	*Amount (weight %)*
Cu	79.9%
O	*20.1%(*)*
**LE (sum)*	*20.1%*

Details of identified phases

A: Copper Oxide Tenorite (100.0 %)*

Formula sum	Cu O
Entry number	96-721-2243
Figure-of-Merit (FoM)	0.764301*
Total number of peaks	190
Peaks in range	190
Peaks matched	21
Intensity scale factor	0.55*
Space group	C 1 2/c 1
Crystal system	monoclinic
Unit cell	a= 4.6837 Å b= 3.4226 Å c= 5.1288 Å β= 99.540 °
I/Ic	4.90
Meas. density	6.450 g/cm³
Calc. density	6.516 g/cm³
Reference	Volanti Diogo P., Orlandi Marcelo O., Andrés Juan, Longo Elson, "Efficient microwave-assisted hydrothermal synthesis of CuO seaurchin-like architectures via a mesoscale self-assembly", 8-15 (1970)

(*)2theta values have been shifted internally for the calculation of the amounts, the intensity scaling factors as well as the figure-of-merit (FoM), due to the active search-match option 'Automatic zero point adaption'.

Search-Match

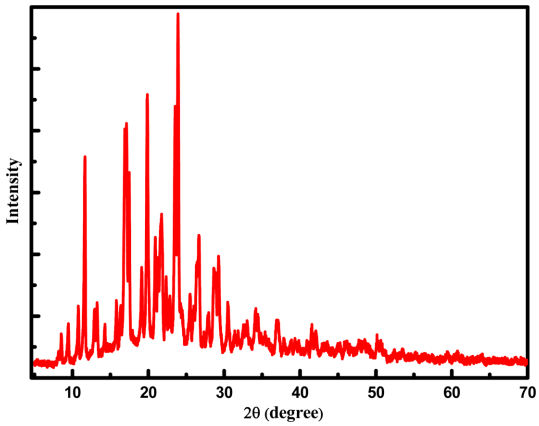

Fig. S2. XRD spectra of HCQ.

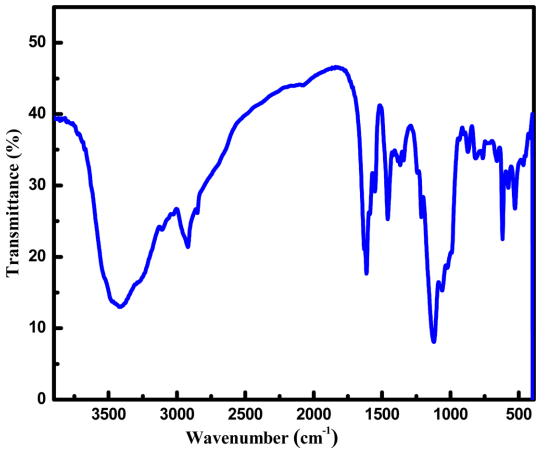

Fig. S3. FTIR spectra of HCQ.

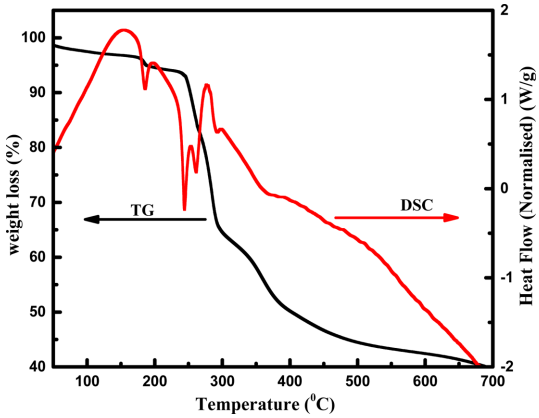

Fig. S4. TG/DSC plot of HCQ.

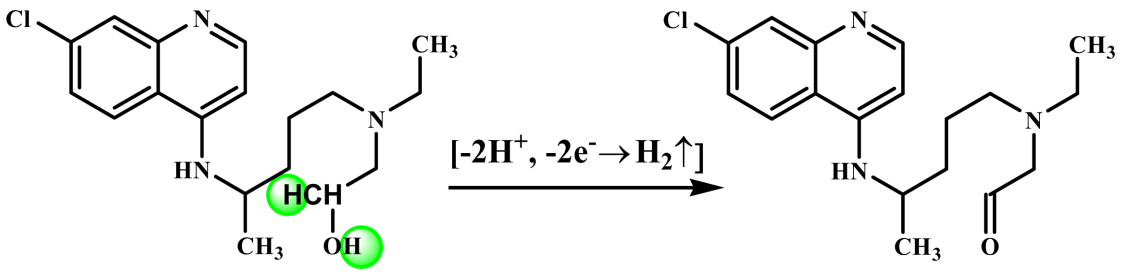

Fig. S5. Electrochemical oxidation mechanism of HCQ for CuO/GO NC/MCPE in 0.1 M PB solution.

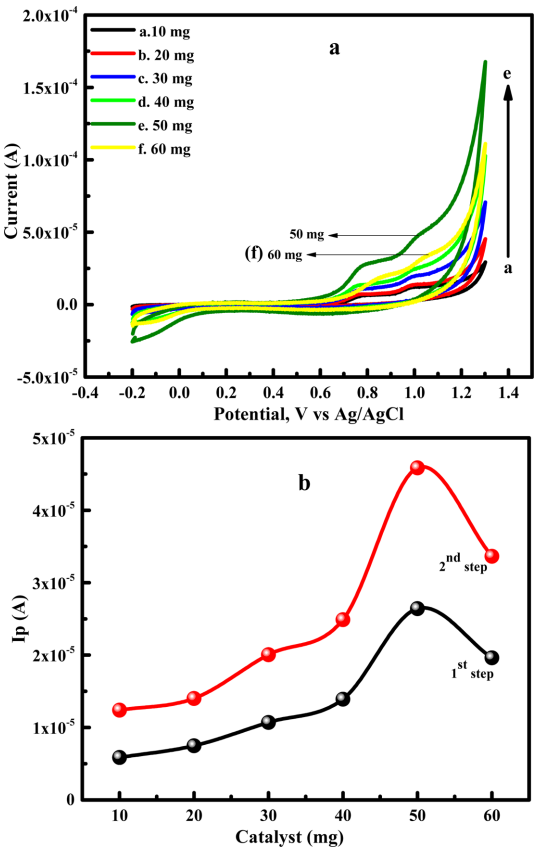

Fig. S6. (a) Variation of the cyclic voltammetric anodic peak current with CuO/GO NC dosages on CuO/GO NC/MCPE in presence of 1 mM HCQ at pH 7 PB, scan rate 100 mV s^{-1}. (b) The first line (black; 1st step) and second line (red; 2nd step) indicates the relationship between I_{pa} *vs.* catalyst dose for the two-step oxidation process of HCQ.

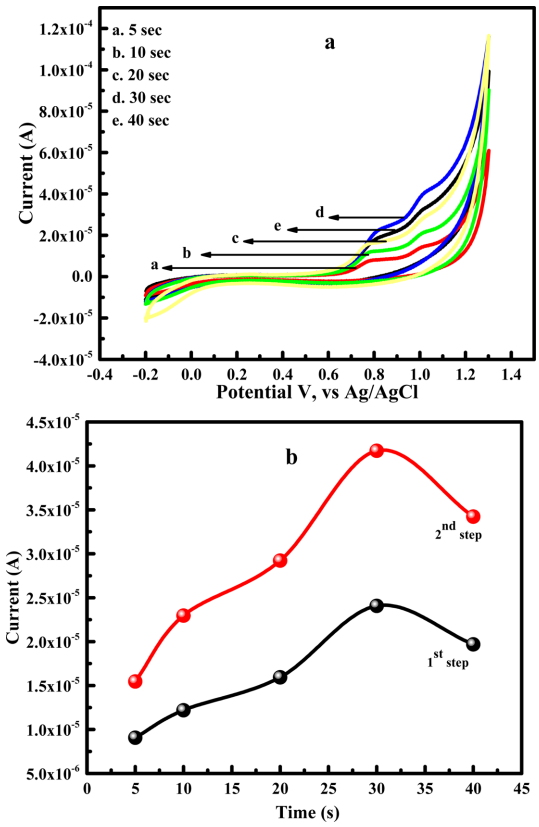

Fig. S7. (a) Variation of the cyclic voltammetric anodic peak current with accumulation time in the presence of 1 mM HCQ at pH 7 PB. (b) The first line (black; 1st step) and second line (red; 2nd step) indicates the relationship between I_{pa} *vs.* accumulation time for the two-step oxidation process of HCQ.

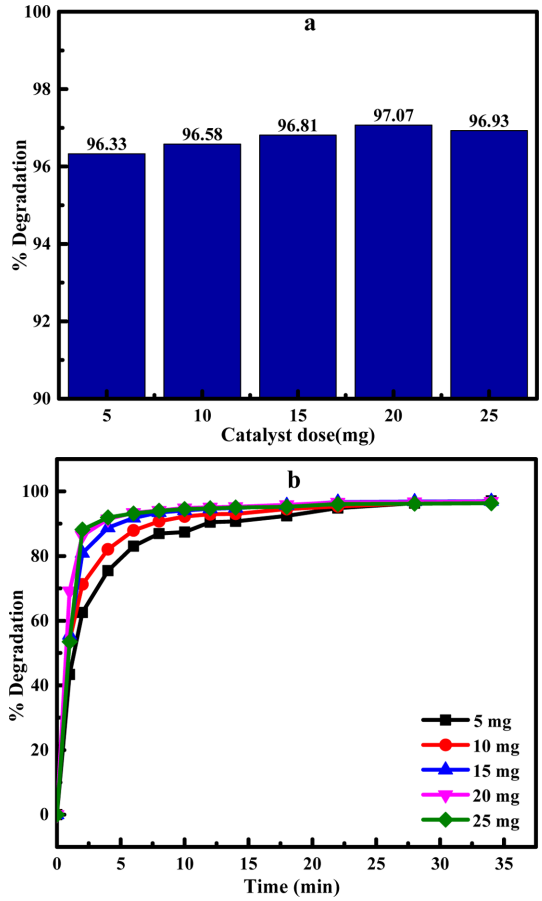

Fig. S8. (a) % degradation of HCQ (0.1 ppm) *vs.* catalyst dose, after 34 min. (b) % degradation of HCQ (0.1 ppm) *vs.* irradiation time.

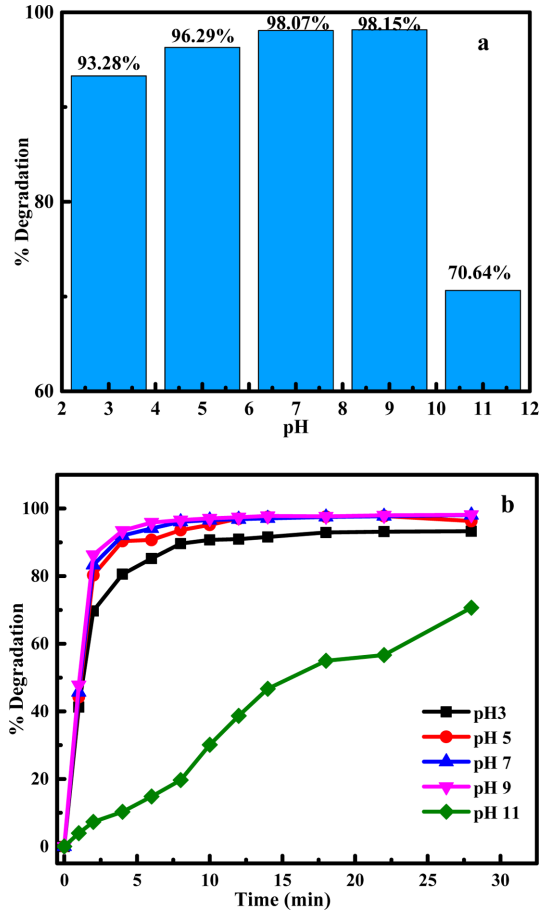

Fig. S9. (a) % degradation of HCQ (0.1 ppm) *vs.* pH (b) % degradation of HCQ (0.1 ppm) *vs.* catalyst dose *vs.* irradiation time at different pH.

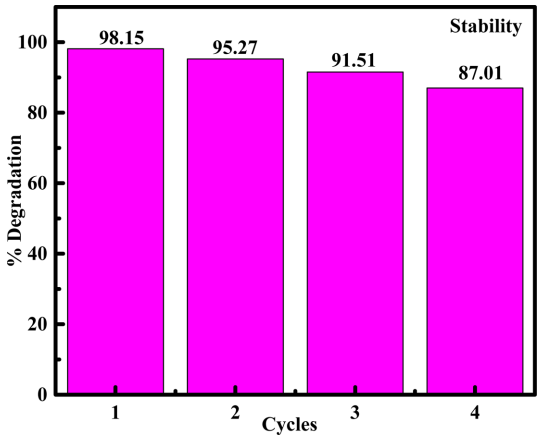

Fig. S10. Photocatalytic stability of CuO/GO NC with HCQ drug.

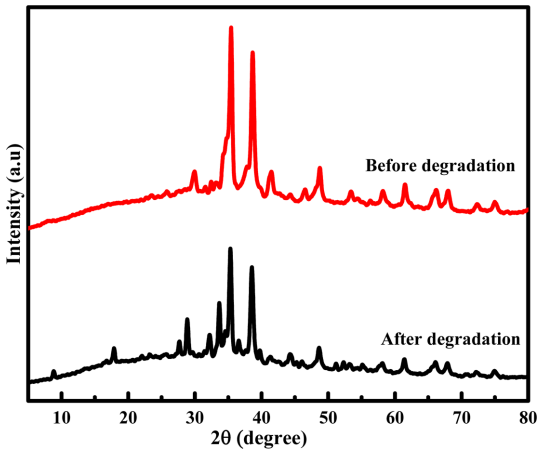

Fig. S11. XRD pattern of fresh and recovered CuO/GO NC after consecutive four cycles.